Remote Sensing of Environment 113 (2009) 1976–1987

Contents lists available at ScienceDirect

Remote Sensing of Environment

journal homepage: www.elsevier.com/locate/rse

Retrieval of snow grain size over Greenland from MODIS

Alexei Lyapustin [a,b,*], Marco Tedesco [b,c,d], Yujie Wang [a,b], Teruo Aoki [e], Masahiro Hori [f], Alexander Kokhanovsky [g]

[a] GEST Center, University of Maryland, Baltimore County, Catonsville, MD 21228, USA
[b] NASA Goddard Space Flight Center, Mail Code 614.4, Greenbelt, MD 20771, USA
[c] City College of New York — CUNY, 138 and Convent Ave., New York, NY 10031, USA
[d] JCET Center, University of Maryland, Baltimore County, MD, 21228, USA
[e] Meteorological Research Institute, Tsukuba, 305-0052 Ibaraki, Japan
[f] Earth Observation Research Center, Japan Aerospace Exploration Agency, 305-8505 Ibaraki, Japan
[g] Institute of Environmental Physics, University of Bremen, O. Hahn Allee 1, D-28334 Bremen, Germany

ARTICLE INFO

Article history:
Received 25 June 2008
Received in revised form 18 May 2009
Accepted 22 May 2009

Keywords:
Snow grain size
Retrieval algorithm
MODIS
Snow melting
Greenland

ABSTRACT

This paper presents a new automatic algorithm to derive optical snow grain size at 1 km resolution using Moderate Resolution Imaging Spectroradiometer (MODIS) measurements. The retrieval is conceptually based on an analytical asymptotic radiative transfer model which predicts spectral bidirectional snow reflectance as a function of the grain size and ice absorption. The snow grains are modeled as fractal rather than spherical particles in order to account for their irregular shape. The analytical form of solution leads to an explicit and fast retrieval algorithm. The time series analysis of derived grain size shows a good sensitivity to snow melting and snow precipitation events. Pre-processing is performed by a Multi-Angle Implementation of Atmospheric Correction (MAIAC) algorithm, which includes gridding MODIS data to 1 km resolution, water vapor retrieval, cloud masking and an atmospheric correction. MAIAC cloud mask is a new algorithm based on a time series of gridded MODIS measurements and an image-based rather than pixel-based processing. Extensive processing of MODIS TERRA data over Greenland shows a robust discrimination of clouds over bright snow and ice. Because in-situ grain size measurements over Greenland were not available at the time of this work, the validation was performed using data of Aoki et al. (Aoki, T., Hori, M., Motoyoshi, H., Tanikawa, T., Hachikubo, A., Sugiura, K., et al. (2007). ADEOS-II/GLI snow/ice products — Part II: Validation results using GLI and MODIS data. *Remote Sensing of Environment*, *111*, 274–290) collected at Barrow (Alaska, USA), and Saroma, Abashiri and Nakashibetsu (Japan) in 2001–2005. The retrievals correlate well with measurements in the range of radii ~0.1–1 mm, although retrieved optical diameter may be about a factor of 1.5 lower than the physical measured diameter. As part of validation analysis for Greenland, the derived grain size from MODIS over selected sites in 2004 was compared to the microwave brightness temperature measurements of SSM/I radiometer which is sensitive to the amount of liquid water in the snowpack. The comparison showed a good qualitative agreement, with both datasets detecting two main periods of snowmelt. Additionally, MODIS grain size was compared with predictions of the snow model CROCUS driven by measurements of the automatic weather stations of the Greenland Climate Network. We found that the MODIS value is on average a factor of two smaller than CROCUS grain size. This result agrees with the direct validation analysis indicating that the snow reflectance model may need a "calibration" factor of ~1.5 for the retrieved grain size to match the physical snow grain size. Overall, the agreement between CROCUS and MODIS results was satisfactory, in particular before and during the first melting period in mid-June. Following detailed time series analysis of snow grain size for four permanent sites, the paper presents maps of this important parameter over the Greenland ice sheet for the March–September period of 2004.

1. Introduction

Snow grain is arguably the most fascinating parameter of a snowpack because of the different geometries that ice grains can exhibit: from large cup shaped grains of depth hoar to stellar flakes characterizing new snow to big structures of grape-shaped rounded crystals of melted/refrozen snow. First observations of snowflakes

* Corresponding author. NASA Goddard Space Flight Center, Mail Code 614.4, Greenbelt, MD 20771, USA.
E-mail address: Alexei.I.Lyapustin@nasa.gov (A. Lyapustin).

0034-4257/$ – see front matter © 2009 Elsevier Inc. All rights reserved.
doi:10.1016/j.rse.2009.05.008

were reported by Kepler (1611) and Descartes (Frank, 1974), the former pondering the question of why the snow crystals exhibit a six-fold symmetry and the latter being the first to provide a morphological description of snow crystals. Later on, in 1665 Robert Hooke (2003) published a volume containing sketches of objects observed with the microscope, including snow crystals. More recently, Wilson A. Bentley (1931) performed microphotography of a large number of snow crystals and Ukichiro Nakaya (1954) conducted their first systematic study. The current methods of studying the shape and size of ice crystals can be found in review by Domine et al. (2008).

Grain size is a fundamental parameter characterizing snowpack properties: for example, the thermodynamic state of a snowpack is related to grain size because of the metamorphism determined by gradients of temperature and vapor; specific snow area and snow diffusivity, which are primary factors in snow chemistry of gases, are related to the snow grain size; spectral snow albedo, playing a key role in the Earth radiation balance, is largely controlled by the grain size (e.g., Domine et al., 2008).

Space-borne remote sensing of the Earth in the visible (~0.4–0.7 μm), near infrared (NIR, ~0.7–1.4 μm) and shortwave infra-red (SWIR, ~1.4–2.5 μm) regions has been used to estimate grain size at large spatial scales and moderate-to-high spatial resolution. In the past 10–15 years, a substantial body of research has accumulated on retrieval of the snow grain size from satellite observations. A comprehensive overview of these works has recently been given by Stamnes et al. (2007). The proposed methods commonly rely on the fact that the absorption of pure ice is very low in the visible, but grows to moderate/strong in the NIR/SWIR (Wiscombe & Warren, 1980). Because ice is highly transparent in the visible, its reflectance has a weak dependence on the grain size and a high sensitivity to absorption by impurities, such as soot. In the NIR region, the ice absorption increases and snow reflectance becomes strongly dependent on the grain size as well as amount of soot. Finally in the SWIR, the ice absorption becomes dominant and snow reflectance depends mainly on the grain diameter.

The retrieval of snow grain size relies on the model of snow reflectance as a function of snow properties, viewing geometry and wavelength. Commonly, Mie (1908) theory has been used for this purpose, and different studies relied on an assumption of spherical particles (e.g., Nolin & Dozier, 1993, 2000; Painter et al., 2003; Stamnes et al., 2007). In the past decade, an analytical asymptotic radiative transfer (AART) snow model was developed which accounts for irregular shapes of snow grains (Kokhanovsky & Zege, 2004; Kokhanovsky et al., 2005, 2006a). Recently, Tedesco and Kokhanovsky (2007) applied AART with the Koch model of fractal particles to derive grain size from the near-infrared measurements of the Moderate Resolution Imaging Spectroradiometer (MODIS). Presented analysis also identified a high sensitivity of retrievals to errors of atmospheric correction. At the same time, the error of cloud detection over snow has by far the largest impact, especially in operational applications.

In this study, we apply a new Multi-Angle Implementation of Atmospheric Correction (MAIAC) algorithm (Lyapustin & Wang, 2009) and AART snow model for the grain size retrieval over the Greenland ice sheet using data collected by MODIS TERRA instrument. An improved knowledge of the temporal evolution of grain size at large spatial scales over Greenland is useful for refining surface melting detection techniques from other satellite data sets (e.g., Tedesco, 2007a) and for understanding how processes such as increased melting (e.g., Tedesco, 2007b) affect the surface energy balance, vertical stratigraphy, and precipitation events (in both timing and extent) over Greenland. Because in situ grain size measurements over Greenland were not available at the time of this work, the MODIS-based results are validated against measurements of Aoki et al. (2007) collected in 2001–2005 in Alaska and eastern Hokkaido, Japan. MODIS-based retrievals were also compared with predictions of a snow model driven with surface meteorological data recorded on ground by the Greenland Climate Network automatic stations.

The paper is structured as follows: Section 2 gives an overview of MAIAC cloud detection and atmospheric correction, and provides detail of the AART snow model. The grain size algorithm is described in Section 3, and Section 4 presents validation analysis. The results obtained from MODIS for selected sites over Greenland and their comparison with predictions of a snow model is discussed in Section 5. This section also provides a qualitative comparison with microwave measurements of the Special Sensor Microwave Imaging (SSM/I) radiometer. Section 6 describes the retrieval results over the Greenland ice sheet for the spring–summer period of 2004. The paper is concluded with the summary.

2. Method description

MAIAC is a new algorithm which uses a time series of MODIS measurements and combines image- and pixel-level processing to detect clouds and perform simultaneous retrievals of aerosol properties and surface bidirectional reflectance and albedo (Lyapustin et al., 2008; Lyapustin & Wang, 2009). The algorithm is generic although the aerosol retrievals are currently not performed over the snow. In this work, we are using a reduced MAIAC processing, which includes cloud mask, water vapor retrievals and a simplified form of atmospheric correction described in Sections 2.1 and 2.2.

2.1. Cloud mask algorithm

The central idea of MAIAC cloud mask algorithm is to build and dynamically update a reference clear-skies image of the surface, which is further used as a comparison target for cloud detection. With a high frequency of global MODIS observations, the land surface can be considered as a static or slowly changing background contrary to ephemeral clouds. In cloud-free conditions, the consecutive images of the same surface area have a well-reproducible spatial pattern and a high spatial correlation. Clouds introduce distortions in this pattern usually in a random way reducing the correlation, which can be detected by covariance analysis. The covariance is a metric showing how well the two images X and Y correlate over an area of $N\times N$ pixels,

$$cov = \frac{1}{N^2}\sum_{i,\,j=1}^{N}\frac{\left(x_{ij}-\bar{x}\right)\left(y_{ij}-\bar{y}\right)}{\sigma_x\sigma_y},\quad \sigma_x^2 = \frac{1}{N^2}\sum_{i,\,j=1}^{N}\left(x_{ij}-\bar{x}\right)^2. \qquad (1)$$

Because covariance removes the average component of the signals, this metric is equally successful over the dark and bright surfaces and in both clear and hazy conditions as long as the surface spatial variability is still detectable from space.

The MAIAC algorithm starts with accumulation of 6–16 days of MODIS data in the processing Queue. The size of the Queue depends on the frequency of MODIS observations over a given location, which is defined by the latitude. MAIAC uses 16 days for the Earth equator where MODIS makes one observation per day, and 6 days for the poles, which feature several orbits per day. For the time series analysis, MODIS data are gridded to 1 km resolution, creating tiles of data.

The covariance analysis is applied for the areas of 25×25 km^2, called blocks, using band 1 (0.645 μm) and band 7 (2.13 μm) data. When the cloud-free conditions for a given block are found, the image is copied to the reference image which is further used to compute covariance with the new MODIS measurements. Each time the new measurements are identified as cloud-free for a given block, the reference image is updated thus dynamically adapting to seasonal variations of the landcover. Similarly, the algorithm dynamically

updates the maximal value and the variance of reflectance in band 1 as well as the brightness temperature contrast ($BT_{max} - BT_{min}$) for each surface block. Analysis of MODIS data shows that thermal contrast is a rather stable metric of a given land area in clear conditions. In partially cloudy conditions, the contrast increases because BT_{min} is usually lower over clouds. This may not be true in polar regions because of frequent temperature inversions in the lower troposphere. In these cases covariance analysis and cirrus test become the main mechanisms to identify cloud-free snow.

The new cloud mask algorithm has an internal surface classifier, producing a dynamic land–water–snow mask, and detecting surface change. These are an integral part of MAIAC guiding the cloud masking when the surface changes rapidly as a result of fires, floods or snow fall/ablation.

The final values of the MAIAC cloud mask are clear, indicating surface type (land, water, or snow) as well, possibly cloudy, and confidently cloudy. The covariance component of the algorithm, which offers a direct way to identify clear conditions, renders another commonly used value of cloud mask — "possibly clear" — redundant. The full description of the algorithm, including the logic of cloud detection at a pixel level, is given in Lyapustin et al. (2008).

The current version of cloud mask algorithm was developed for generic land applications. It may need further enhancements for Arctic, such as discrimination of the sea ice. Nevertheless, we found that it has a good performance over the snow detecting significantly more clear snow pixels than the operational MODIS cloud mask algorithm MOD35 (Lyapustin et al., 2008).

An example of *MAIAC* cloud mask for Thule located on the northwest of Greenland (77°30′N, 69°10′W), is shown in Fig. 1. It shows 6 consecutive daytime MODIS TERRA gridded images for two days 112–113, 2004, for 150×150 km^2 area. The daytime conditions are defined according to solar zenith angle of less than 75° (see Section 3). Two left columns show the TERRA RGB images. They are differently normalized to help distinguish clouds from the bright snow. The central feature in the image shows a fiord covered by snow/ice, which melts in the summer.

The third column shows the derived cloud mask, which uses the following legend: red — cloud; white, blue and light blue — clear over snow, land and water, respectively. A reproducible spatial pattern helps to identify cloud-free blocks of the surface. The top three images represent the clear-skies conditions. The second image is obtained near the edge of scan and has an apparently coarser resolution than images 1 and 3 acquired close to nadir. Clouds are seen in the images 4–6 as distortions to the spatial pattern of reflectance. For the most part, they are captured by the cloud mask algorithm.

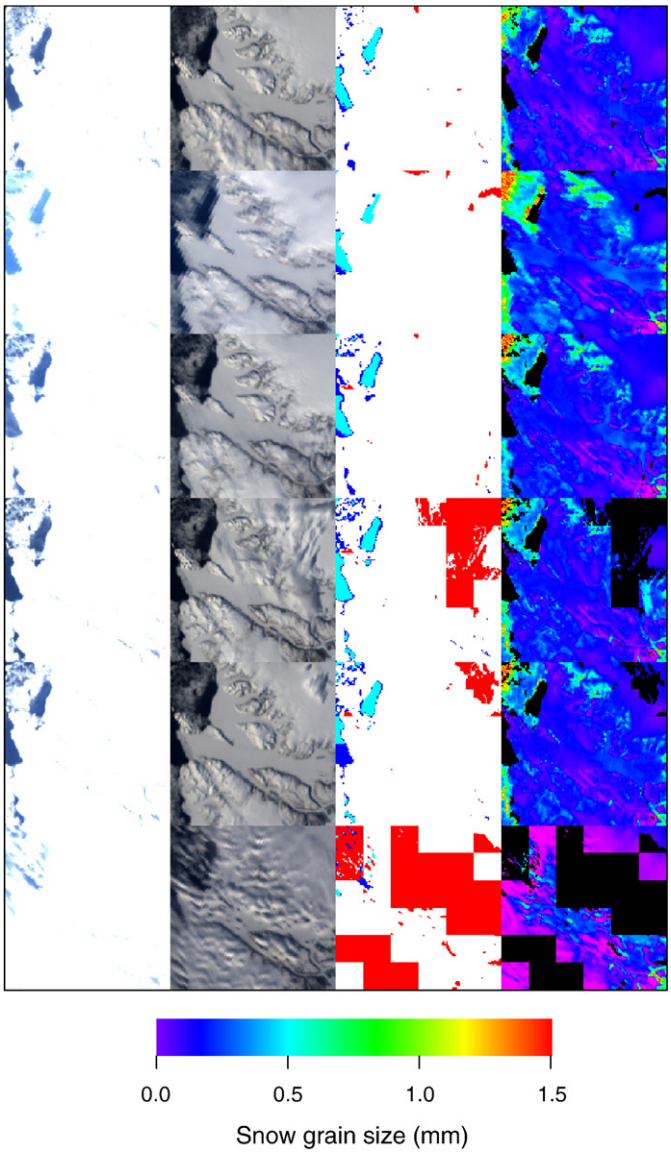

Fig. 1. Illustration of MAIAC cloud mask for all consecutive MODIS TERRA observations over Thule, Greenland (the area of 150×150 km^2) for two days 112–113 of 2004. The left two columns show the RGB image of gridded MODIS L1B data. They are normalized differently to help distinguish clouds over the snow. The third column shows MAIAC cloud mask, which uses the following legend: red — cloud; white, blue and light blue — clear over snow, land and water, respectively. The last column shows the retrieved snow grain diameter (see Section 3).

2.2. Atmospheric correction of MODIS data

The aerosol concentration over Greenland is generally low (Tomasi et al., 2007) except events of transported biomass burning smoke or pollutions from Northern America or Eurasia. Because of high surface reflectivity and cloud contamination, reliable remote sensing methods for aerosol retrievals over this region of the world do not exist. For these reasons, we are using a low constant value of background aerosol optical depth τ^a (0.55 μm) = 0.02. Our sensitivity analysis showed that over bright Arctic snow/ice, an uncertainty in the knowledge of aerosol optical depth of ±0.02 has no practical effect on results of a band-ratio algorithm of snow grain size retrievals used in this work (see Section 3). In other respects, MAIAC makes a full correction of effects of Rayleigh scattering and molecular absorption including absorption by water vapor and ozone.

Table 1 shows the effective center wavelengths of MODIS TERRA 500 m bands, the in-band optical thickness of absorption by well-mixed gases and by water vapor at the column amount of 1 cm. The effective band center wavelength is defined as a wavelength for which monochromatic and narrow-band direct vertical transmittances of the aerosol-free atmosphere are equal:

$$\exp\left\{-\tau^R(\lambda_C)\right\} = \int_{\Delta\lambda} F_\lambda \exp\left\{-\tau^R(\lambda)\right\} h_\lambda d\lambda \Big/ \int_{\Delta\lambda} F_\lambda h_\lambda d\lambda, \quad (2)$$

where F_λ is extraterrestrial spectral solar irradiance, h_λ is relative spectral response function of MODIS TERRA bands, and τ^R is Rayleigh optical thickness computed with model of Bodhaine et al. (1999). The optical thickness of the in-band gaseous or water vapor absorption is defined similarly. The optical thickness of absorbing gases is calculated for the carbon dioxide concentration of 380 ppm, and concentration of other gases corresponding to the Arctic atmospheric model (Kneizys et al., 1996). The calculations included absorption of 6 major atmospheric gases (H_2O, CO_2, CH_4, NO_2, CO, N_2O) with line parameters from HITRAN-2000 (Rothman et al.,8 2003) database using the Voigt

Table 1
The center wavelength of MODIS TERRA land 500 m channels, the in-band absorption optical thickness of well-mixed gases and of 1 cm of water vapor, and effective refractive index of ice.

Band N	B1	B2	B3	B4	B5	B6	B7
λ_C, μm	0.6449	0.8556	0.4655	0.5535	1.2419	1.6290	2.1131
τ^g	1.32e−3	1.82e−5	2.06e−3	4.60e−4	2.90e−3	1.01e−2	1.80e−2
τ^w, 1 cm	3.62e−3	5.49e−3	5.20e−5	3.63e−4	3.62e−3	0.87e−3	1.63e−2
$\bar{\chi}_e^{ice}$	1.25e−8	2.32e−7	1.05e−9	3.22e−9	1.20e−5	2.41e−4	(5.3–6.8)e−4

vertical profile, and the Atmospheric Environmental Research continuum absorption model (Mlawer et al., in preparation).

The top-of-atmosphere reflectance is modeled in this work using a modified Lambertian formulation under an assumption that most of the ozone absorption takes place above the molecular atmosphere:

$$R_{\Delta\lambda}(\mu_0,\mu,\varphi) \cong \left(R^A_{\Delta\lambda}(\mu_0,\mu,\varphi) + \frac{\rho(\mu_0,\mu,\varphi)T_{\Delta\lambda}(\mu_0,\mu)}{1-q(\mu_0)s_{\Delta\lambda}}\right)T^{Ozone}_{\Delta\lambda}(\mu_0,\mu). \quad (3)$$

Here, R^A is atmospheric path reflectance, T is a total upward and downward atmospheric transmittance, s is spherical albedo of the atmosphere, ρ and q are surface bidirectional reflectance factor and albedo, respectively. μ_0, μ, φ stand for cosines of solar and view zenith angles, and relative azimuth. The subscript indicates that the functions are weighted with respective spectral response of MODIS channels:

$$R_{\Delta\lambda} = \int F_\lambda R_\lambda h_\lambda d\lambda \Big/ \int F_\lambda h_\lambda d\lambda. \quad (4)$$

Because atmospheric optical thickness over Greenland is low, correction using Lambertian Eq. (3) is rather accurate even at relatively large sun zenith angle (Lyapustin, 1999). The atmospheric correction is based on the look-up table computed using radiative transfer code SHARM (Lyapustin, 2005) and the Interpolation and Profile Correction method (Lyapustin, 2003) for narrow-band and shortwave broadband calculations.

After generating cloud mask, MAIAC retrieves column water vapor with a relative accuracy of 5–10% from MODIS NIR channels 17–19 located in the water vapor absorption band 0.94 μm using a band ratio technique (Lyapustin & Wang, 2008). The retrieved values over Greenland for the period covering spring to fall of 2004 agree well with known climatology (Kneizys et al., 1996) showing the average values of 0.2–0.4 cm for the spring and autumn, and 0.4–0.8 cm for the summer period.

Because of significant surface height variation over Greenland, the height/pressure correction is implemented for functions R^A, T and s in the visible and near infrared bands 1–4 as described in (Lyapustin & Wang, 2008).

2.3. Snow reflectance model

In this work, we are using the AART model of snow reflectance developed by Kokhanovsky and Zege (2004). This model predicts snow reflectance using an asymptotic analytical solution of the radiative transfer problem in semi-infinite media with low absorption (the so-called Milne problem), which is a good approximation for snow in the visible spectral range:

$$\rho = R_0(\mu_0,\mu,\varphi)\exp\left(-A(\mu_0,\mu,\varphi)\sqrt{\gamma d}\right). \quad (5)$$

Here, $\gamma = 4\pi\chi/\lambda$, χ is imaginary part of refractive index of ice, λ is wavelength, and $d = 6\langle V\rangle/\langle S\rangle$ is an effective grain size defined by ratio of the average volume to the average surface area of grains. R_0 is a solution of radiative transfer equation for snow with zero absorption. For simplicity, we assume that R_0 does not depend on snow grain size because the wavelengths at consideration (0.4–2.1 μm) are much smaller than parameter d, which is known to vary from about 50 μm for fresh snow to 1–1.5 mm in pre-melting conditions (Wiscombe & Warren, 1980) to several millimeters during snowmelt. The function A relates to the photon's escape probability from the media. For the fractal ice particles, it can be approximated as follows:

$$A(\mu_0,\mu,\varphi) \cong K(1+2\mu_0)(1+2\mu)/R_0(\mu_0,\mu,\varphi), \quad (6)$$

where K is the calibration constant depending on the type of snow. It equals approximately to 0.66 for fractal snow grains (Kokhanovsky & Zege, 2004). Comparison of described analytical model with an accurate radiative transfer solution showed the accuracy of better than about 3% for zenith angles below ≈78°. A local model validation with field measurements has demonstrated a good angular and spectral agreement in the range 0.535–2.21 μm (Kokhanovsky et al., 2005).

The described snow reflectance model has several limitations. First, as we mentioned, the zenith angles cannot be too high, which may limit retrievals over polar regions in winter, early spring and late fall when solar zenith angle is low. Second, comparisons with measurements showed that the model is not applicable near the forward scattering (glint) direction ($\varphi \sim 0°$). Third, the model was derived with the assumption of low absorption, $\beta = \sqrt{\gamma d} \ll 1$. This assumption holds well for MODIS vis-NIR bands 1–5, but in the shortwave infrared region for bands 6 (1.6 μm) and 7 (2.1 μm) parameter β may be as high as 0.5–1 during snowmelt. On the other hand, ground-based measurements of the bidirectional reflectance of snow (Kokhanovsky et al., 2005) and processing of AATSR data (Kokhanovsky & Schreier, 2009) showed that the model can be used in the SWIR region as well.

In general, the snow model should include light absorption by liquid water in snow (Green et al., 2002) and by absorbing impurities, such as soot from biomass burning and urban-industrial aerosols (Warren & Clarke, 1986) or transported dust. In this work, however, we did not find evidence from MODIS data of measurable soot contamination over Greenland in 2004, at least above sensitivity of our model. Our analysis also showed that adding water absorption has almost no effect in the MODIS bands used for the grain size retrievals because the imaginary part of the refractive index is nearly the same. For these reasons, we decided not to consider these sources of absorption further.

Besides absorption, the presence of liquid water in the snow pack may significantly increase an apparent optical grain size related to snow reflectance (e.g. Chylek et al., 2007). Displacing the interstitial air, the liquid water may make multiple ice grains appear as one large grain in the reflected light, whereas the physical size of grains may not have changed much. In terms of the radiative transfer, this would affect density of scatterers and their vertical profile, single scattering albedo and an asymmetry parameter of scattering. This example shows that interpretation of theoretical 'radiative diameter' and its relation to the physical grain size may be very complex especially in melting conditions.

An obvious advantage of the AART model is an explicit dependence on the grain size and snow refractive index. This offers a straightforward and very effective inversion scheme, which would only require tabulating function R_0 as a function of angles. For this work, the look-up table of function R_0 was computed with the radiative transfer code SHARM (Lyapustin, 2005) using the scattering function for random

fractal crystals (Mishchenko et al., 1999). Mishchenko provides 2000 Legendre expansion coefficients. We found that SHARM solution achieved convergence with an accuracy of about 0.1–0.2% when we used 1024 coefficients.

The last row of Table 1 shows the band-average imaginary part of an in-band effective refractive index of ice $\bar{\chi}_e^{ice}$ based on the latest compilation of Warren and Brandt (2008), which is computed from equation

$$\exp\left(-A(\mu_0,\mu,\varphi)\sqrt{\frac{4\pi\bar{\chi}_e^{ice}d}{\lambda_C}}\right) = \int \exp\left(-A(\mu_0,\mu,\varphi)\sqrt{\frac{4\pi\chi^{ice}(\lambda)d}{\lambda}}\right)F_\lambda h_\lambda d\lambda \Big/ \int F_\lambda h_\lambda d\lambda. \quad (7)$$

The effective value accounts for spectral variations of $\chi^{ice}(\lambda)$ within the band-pass interval, for variations of function $A \cong 0.4–2.2$ with the MODIS viewing geometry, and for changes of diameter during snowmelt. We found that using effective values improves spectral agreement between the model and the MODIS measurements in the NIR and SWIR bands.

3. Method of grain size retrieval

The developed algorithm has several processing stages: a) gridding MODIS level 1B geolocated and calibrated data to 1 km resolution; b) retrieving water vapor; c) cloud masking; d) performing atmospheric correction; e) retrieving snow properties.

The snow grain size can be derived from satellite data using either a single channel (e.g. Nolin & Dozier, 1993; Stamnes et al., 2007) or often used band-ratio algorithms (e.g., Scambos et al., 2007). The first approach requires an accurate knowledge of the bidirectional reflectance R_0. We analyzed the accuracy of the modeled function R_0 experimentally by comparing it with atmospherically corrected MODIS TERRA reflectance for the full range of daytime viewing geometries and conditions during 7 months (March–September) of 2004 over Greenland. The day time conditions below are defined according to solar zenith angle <75°, where limitation is set from several considerations: 1) to conform with validity range of the AART model; 2) to limit the effect of anisotropic snow reflectance on the grain size retrievals; and 3) this is the range where the plane-parallel radiative transfer model used for atmospheric correction remains valid, whereas distortions caused by sphericity of Earth's atmosphere become important at higher zenith angles. Fig. 2 shows a comparison

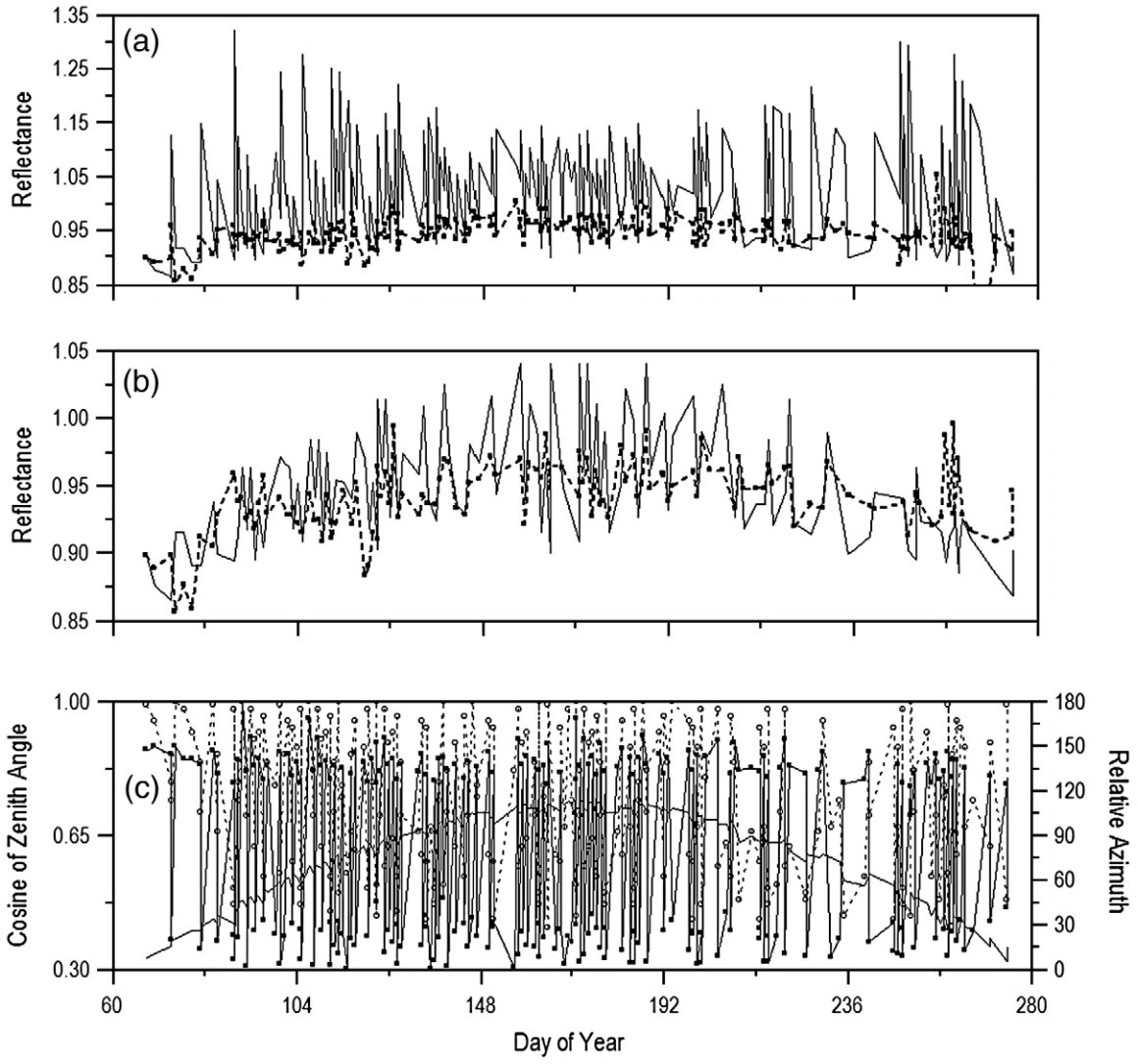

Fig. 2. Comparison of function R_0 (solid line) with atmospherically corrected MODIS TERRA reflectance in the blue band (0.47 μm) for the Saddle site for the period of March to September 2004. The top figure (a) shows the full set of clear-skies measurements at solar zenith angle below 75°. The middle figure (b) shows the reduced dataset with forward scattering directions ($\varphi \leq 40°$) filtered. The bottom plot (c) shows the geometry of observations for the full set of measurements. The smooth solid line and dashed line with circles show the cosine of solar and view zenith angles, respectively. The rapidly changing solid line with filled box symbols shows the relative azimuth.

for the Blue (B3) band for the cloud-free observations as detected by MAIAC cloud mask for the Saddle site (66.0006N, 44.5014W). Fig. 2a shows results for all view angles with geometry plotted in the bottom Fig. 2c. The spikes of function R_0 correspond to the glint directions where the AART model is not valid. It is interesting that MODIS measurements do not show significant increase of reflectance in the forward scattering directions. This result is typical not only for this particular site but for the full area of Greenland. Fig. 2b shows a reduced set of measurements where azimuthal angles $\varphi \le 40°$ were filtered. Although the agreement in this case is significantly better, the MODIS reflectance still shows less anisotropy than theoretical predictions. The main reason for this disagreement is a macroscopic surface roughness caused by the local terrain variations (slope and height variations), sastrugi, etc. There is a significant amount of such variability inside 1 km grid cell which flattens the anisotropy of reflectance and which is not taken into account by the plane-parallel radiative transfer model used to compute R_0 (e.g., Hudson et al., 2006; Hudson & Warren, 2007). Nolin and Payne (2007) used MISR data to classify surface roughness in glacial zone of Western Greenland.

For this reason, we selected the band-ratio algorithm where the role of function R_0 is reduced to the second-order effect manifested through function A. Using two channels with different ice absorption, it is easy to obtain from Eq. (5):

$$d = \frac{1}{4\pi A^2}\left[\ln\left(\frac{\rho_1}{\rho_2}\right) / \left(\sqrt{\chi_2/\lambda_2} - \sqrt{\chi_1/\lambda_1}\right)\right]^2. \quad (8)$$

Because of R_0, there is some uncertainty in the magnitude of function A in Eq. (8), which may introduce some bias in parameter d. Since this function depends only on the viewing geometry, the possible bias should not affect spatial variations of derived grain size. The calibration of the retrieved d with ground-based measurements can be used to improve the model of function A (see Section 5). Some preliminary results on such experimental calibration have been reported by Kokhanovsky (2006b).

Eq. (8) is valid for the case of vertically homogeneous snow with small wavelength separation when the light penetration depth in snow is similar between the two wavelengths. When snow is inhomogeneous, d represents a value averaged over the penetration depth. In this case, it is important to use a combination of non-absorbing channel (1) with absorbing channel (2). Then it follows from Eq. (8):

$$d = \frac{\lambda_2}{4\pi\chi_2 A^2}\ln^2\left(\frac{\rho_1}{\rho_2}\right). \quad (9)$$

This equation was used in our algorithm with $\lambda_1 = 0.645$ μm and $\lambda_2 = 1.24$ μm. The example of retrieved grain size using the ratio $\rho_{0.65}/\rho_{1.24}$ is shown in the last column of Fig. 1. Gridding allows an easy comparison between successive observations of the same area. The spatial pattern of the grain size is reproduced consistently for different observations on a single day and on consecutive days. The residual dependence on the view zenith angle and on azimuth is small. In these retrievals, the forward scattering directions $\varphi \le 40°$ were excluded.

A time series of retrieved grain size for the Saddle site is shown in Fig. 3. Here, we used several different ratios created from bands 1 (0.645 μm), 2 (0.87 μm), and 5 (1.24 μm). The ratios ρ_1/ρ_5 and ρ_2/ρ_5 produce essentially the same results showing very stable retrievals in the absence of melting and a similar growth of grain size during the two periods of snowmelt. Another ratio ρ_1/ρ_2 (red line) used by Scambos et al. (2007) has a good sensitivity during snowmelt periods but produces unstable results for the other periods with values often below 50 μm. This result suggests that the difference in the ice absorption between the Red and NIR (band 2) bands may insufficient for reliable retrievals outside of melting periods when the grain size remains relatively small.

The R6 line shows grain size retrieved using Eq. (5) from a single band 6 (1.64 μm) where the ice absorption is high. A similar approach was used in retrievals of Stamnes et al. (2007) from data of Global Imager (GLI) flown onboard of ADEOS-II satellite. In complete agreement with results from the above reference, this retrieval shows smaller d-values as compared to shorter wavelengths. The higher values of the retrieved grain size at shorter wavelengths are usually explained by a larger depth of penetration of light into the icepack (e.g. Li et al., 2001) and growth of the effective grain size with depth (Grenfell et al., 1994; Aoki et al., 2000).

Further, the ratio R_5/R_1 will be used as a baseline for our retrievals. In order to assess sensitivity of this method, the retrievals were conducted for different sites in the inland Greenland and compared with outputs of a snow energy balance model as well as with trends of space-borne microwave brightness temperature, which is described in Section 5. Independently, we studied behavior of grain size in the coastal regions of Greenland characterized by persisting melting and variations due to re-freeze and/or new snowfall. Fig. 4 shows retrievals for the glacial area north-east of Thule shown by a red circle in the top-left image of Fig. 4. The retrieved diameter is an average for the cloud-free pixels over an area of 5×5 km^2. There are several pronounced periods of systematic growth, followed by a sharp drop. Some of these are selected by ovals in the figure. We have looked at periods 1 and 2 in detail trying to identify whether this is an uncertainty of solution or it relates to a change of the snow state. In both cases, the decrease of grain size was preceded by a period of cloudiness. It also correlates with decrease of the measured SSM/I brightness temperature. The spatial RGB images are shown next to the time series of grain size. We cannot provide much detail on the state of snow for the first period (days 134–136). The retrievals show high

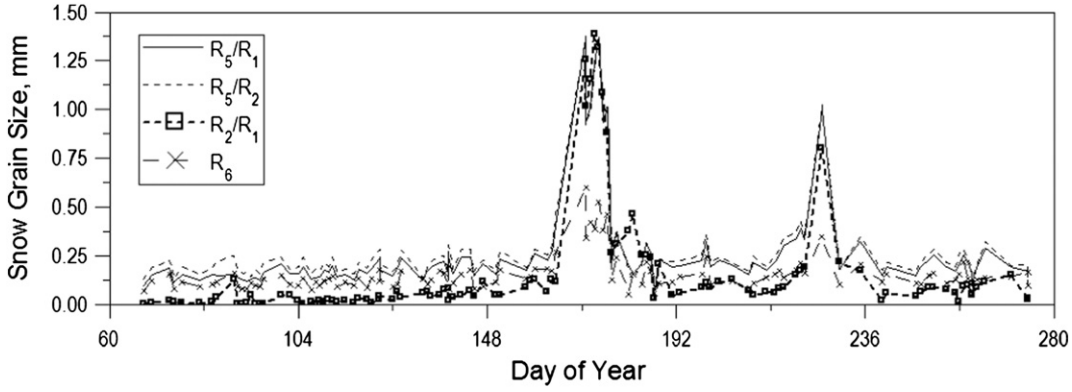

Fig. 3. A time series of the derived snow grain size over Saddle, Greenland, for the period of March–September 2004. The retrievals used the following channels: B1 (0.645 μm), B2 (0.87 μm), B5 (1.24 μm), B6 (1.64 μm).

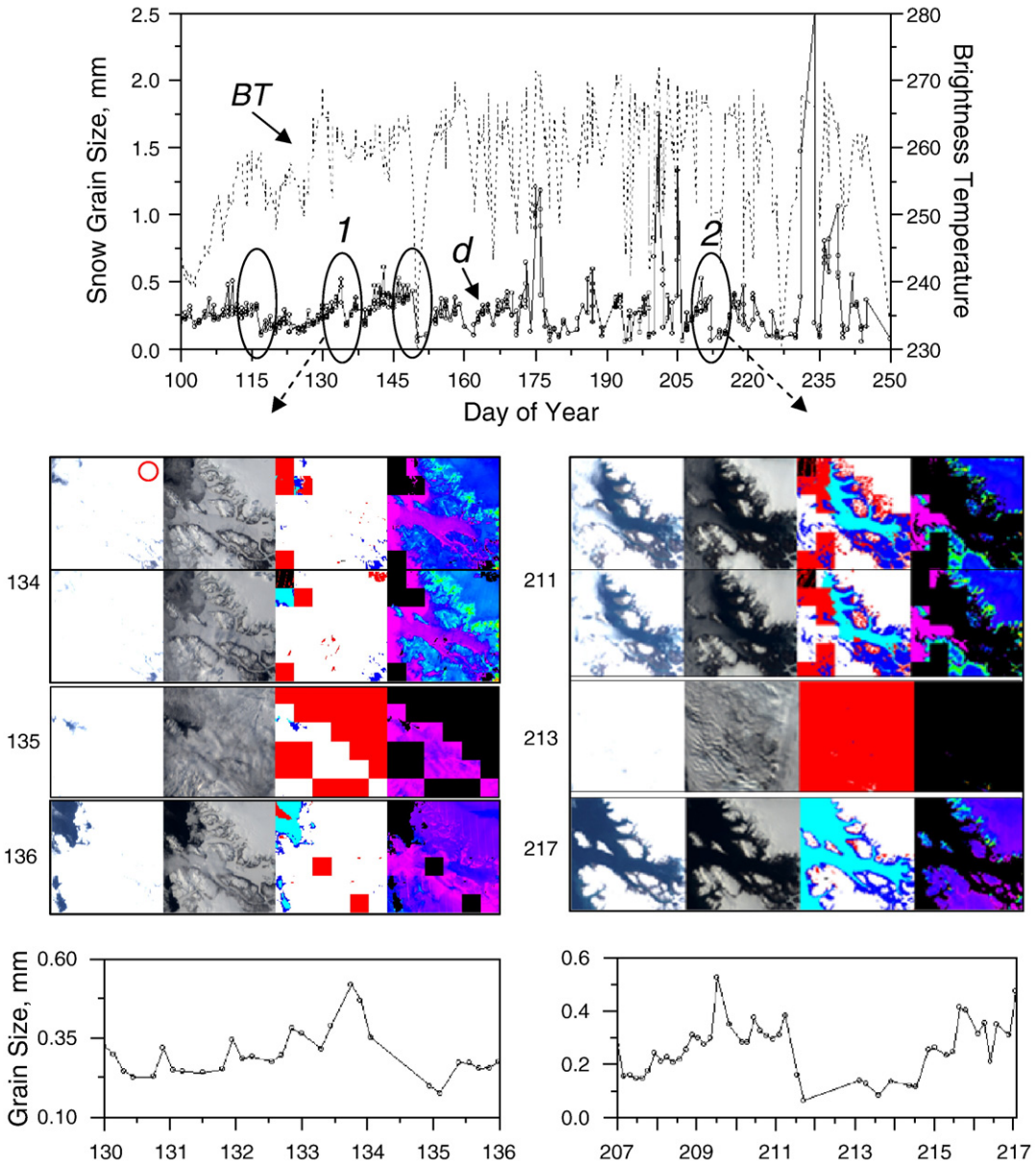

Fig. 4. (Top) A time series of retrieved snow grain diameter (d) and brightness temperature (BT) for the area shown by a red circle near Thule, Greenland in 2004. (Middle) MODIS TERRA RGB images, cloud mask, and retrieved snow grain size for the periods 1 (days 134–136) and 2 (days 211–217) for the area of 150×150 km^2 at resolution of 1 km. (Bottom) Expanded time series of retrieved grain size for periods 1 and 2.

values $d=0.5$–0.52 mm on day 134. After the cloudy day 135, the days 136–137 were completely cloud-free, and the retrieved value was systematically lower ($d\sim0.22$–0.3 mm). It was slowly growing back to the range of $d\sim0.5$ mm during the next cloud-free period on days 139–144.

On the second period (days 211–217), there was a fresh snowfall during the extended 6-day period of complete or partial cloudiness accompanied by the decrease of retrieved grain size. On day 211 and on the morning of day 212, a snow-free land is clearly visible along the border of the fiord, and the average retrieved snow diameter was 0.38 mm. The area was mostly covered by clouds from the mid-day 212 through mid-afternoon of day 216. After that, most of the bare land can be seen as covered by a new snow, shown on image for day 217. After cloud passing, the average diameter decreased to $d=0.22$–0.25 in the afternoon of day 216. The retrievals on partially cloudy days 212, 214 and 215, showing values $d\sim0.12$ mm, may be biased low by undetected or sub-pixel clouds which remains the main problem of the automated algorithms of the remote sensing of snow properties. For example, three 25 km blocks next to the upper-right corner are likely to be contaminated by clouds resulting in low grain size values.

Even with our restriction on solar zenith angle ($\leq75°$), MODIS TERRA provides 4 to 5 observations per day over Thule. With changing view geometry, the effect of snow bidirectional reflectance becomes important. It causes daily retrieval "spikes" clearly visible in the bottom left plot of Fig. 1. Each of them corresponds to a high view zenith angle over 50–55°. For example, the highest value $d=0.52$ mm corresponds to MODIS measurements acquired at solar angle 62°, view zenith angle 63.9° and relative azimuth 121°. Because plane-parallel radiative transfer cannot capture snow anisotropy well, this effect was cited by Aoki et al. (2007) as one of error sources of the GLI snow algorithm. In our case, the use of band ratio substantially mitigates this error but cannot exclude it entirely. For the case shown in Fig. 1, we can assess the error of a single measurement as 0.05–0.06 mm. At the same time, these errors can be filtered in the time series post-processing because the grain size retrievals are rather consistent at lower view zenith angles.

These examples show that the developed method is sufficiently sensitive to detect melting and fresh snowfall. It may also be sensitive to some forms of snow metamorphism (Colbeck, 1983), including refreeze. To understand sensitivity and limitations of the proposed method quantitatively, a continuous ground-based measurement of snow grain size is needed in summertime in the glacial area with pronounced temporal variability of snow properties.

4. Grain size validation

Because in-situ data for Greenland were not available at the time of this work, we are using snow pit measurements by Aoki et al. (2007) collected as part of the GLI validation campaign. The field data were collected in 2001–2005 at Barrow site (Alaska) and at three sites in eastern Hokkaido, Japan, located in the Saroma lagoon, Lake Abashiri and Nakashibetsu area. All sites are topographically flat. The Saroma site was a snow-covered lagoon. The field experiments, made in February of 2001 and 2002, represent dry snow at the surface, such as new snow and faceted crystals, with the lower layers consisted of depth hoar and granular snow. The snow was 7 to 31.5 cm deep overlying stable and flat lagoon sea ice. The Barrow site was tundra covered by 21–33 cm deep snow, which at the surface was similar to that at the Saroma site but with the underlying layers of depth hoar. The field measurements were made in April 2003. The Abashiri site was lake ice covered by 17 cm of wet granular snow, and field data were collected in March 2004. The Nakashibetsu site was a flat, snow-covered farmland and the field measurements were made in March 2004 and 2005. In 2004, the snow conditions were wet granular snow with sun crust and a depth ranging from 92 to 106.5 cm. In 2005, the surface snow condition was compacted snow and the lower layers consisted of depth hoar and granular snow. The snow depth was 79 cm.

The snow grain size was measured with a handheld lens by the method described by Aoki et al. (1998, 2000). The earlier works of Aoki et al. (1998, 2000) showed that the optically equivalent snow grain size for a new snow or faceted crystals (lightly compacted snow) corresponds to the branch width of dendrites or the width of a narrower portion of broken crystals (parameter d_2). The current comparison is performed against measured diameter d_2. The uncertainty of Aoki's data was evaluated as $\pm$0.01–0.02 mm.

For this comparison, we used measured data within $\pm$2 h of MODIS TERRA and AQUA overpass. In the visible range (0.4–0.8 μm), the snowpack attains properties of a semi-infinite layer at depths varying from about 20 cm for a new (fine grained) snow to about 50 cm for an old snow (e.g., Wiscombe & Warren, 1980; Zhou et al., 2003). For reference, grain size retrievals from GLI were performed using wavelength of 0.9 μm, and validation analysis of Aoki et al. (2007) was performed against measurements averaged over the top 5 cm layer. Snow becomes moderately absorptive at the reference wavelength of 1.24 μm used in our retrievals, which reduces penetration depth. Our assessments of photon depth penetration (defined as a depth at which radiative flux is reduced by a factor of e) based on SHARM simulations gave results similar to those of Li et al. (2001), namely from ~0.55 cm for 100 μm grains to ~1.3 cm for 500 μm grains at $\lambda = 1.24$ μm. Here, we assumed spherical particles and a grain concentration of 0.3. The result of comparison is shown in Fig. 5 (left). We used measured grain diameter in the top 0–1 cm layer which agrees with theoretical estimates of penetration depth, and used only cases with total snow depth exceeding 5 cm. We did not separate cases of dry and wet snow because validation points do not show separable behavior. Given the uncertainties of measurements, the overall agreement is good.

The cluster of points in the left image marked by ovals was collected over Barrow site on April 26, 2003. The measurements were performed on a cross shape in five 1 km grid points. The collected data were highly inhomogeneous due to crust in the top 0.5 cm layer. For example, measured parameter d_2 in the top layer was 1.3 mm in the north pit and 0.8 mm in the center, and was relatively homogeneous ($d_2 = 0.15$–0.2 mm) in the other three pits. At the same time, MODIS retrievals agreed very well between the 5 grid points, including an excellent agreement between TERRA and AQUA within $\pm$0.05 mm. The average value from MODIS is 0.36 ± 0.04 mm where the uncertainty covers the full range of variation. This result indicates that Barrow site could be very inhomogeneous due to presence of crust at small scales affecting pit measurements, and rather homogeneous at a scale of 1 km of our retrievals. Assuming that five pit points more or less adequately represent spatial distribution of snow grain size in the top layer at a larger scale, we can average collected data. The averaging gives the value of $d_2 = 0.35$ mm which agrees well with both individual and an average (0.36 mm) MODIS retrieved values. The inhomogeneity of the Barrow site and of Nakashibetsu location (due to presence of sun crust) was discussed at length by Aoki et al. (2007), who also raised the question of spatial representativeness of the ground measurements.

The new plot where the Barrow measurements are represented by a single average value is shown in the right Fig. 5. One can see that the regression improved significantly: the correlation coefficient increased from $R^2 = 0.46$ to $R^2 = 0.60$, the slope improved from 0.47 to 0.65, and the offset decreased by a factor of 4. We may draw a preliminary conclusion from Fig. 5 (right) that in order to achieve 1:1 agreement between retrievals and measurements, the optical snow model used here may need a calibration factor of up to 1.5. The presented discussion also shows the need for spatially representative

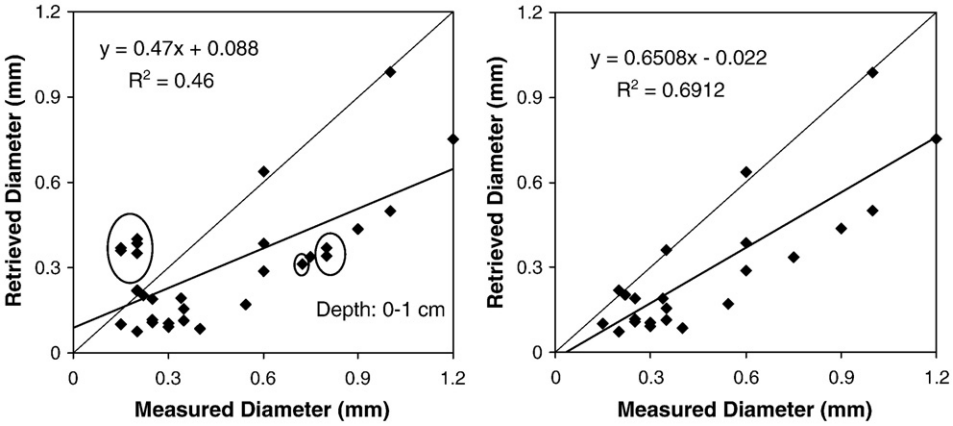

Fig. 5. Comparison of retrieved snow grain diameter with measured diameter averaged over the top 0–1 cm layer. In the right image, the cluster of points corresponding to measurements over Barrow, Alaska, and indicated by oval shapes, is represented by a single averaged value.

statistics of ground validation measurements which could provide a better accuracy for the model calibration. The future experiments could greatly benefit from a preliminary reconnaissance of the validation sites using a combination of moderate and high resolution spaceborne (or airborne) measurements. This could help to either identify locations where snow properties remain homogeneous at a scale of several satellite footprints, or find a scale of inhomogeneity inside footprint to help select the grid distance for the ground measurements.

5. Comparisons with snow model outputs and microwave data

In this section, grain size values retrieved with MODIS are evaluated versus those simulated with a snow physical model CROCUS (Brun et al., 1989, 1992). Snow grain in CROCUS is defined in terms of optical size for albedo computation and physical size for stability assessment (Brun et al., 1992). Following initialization, the grain size evolution is computed according to the forcing data. Here, forcing to the CROCUS model is derived from measurements of the automatic weather stations of the Greenland Climate Network (Steffen et al., 1996).

Beside the results from CROCUS, a qualitative analysis of the MODIS-retrieved grain size is also performed using data of the Special Sensor Microwave Imaging (SSM/I) radiometer. The microwave brightness temperature at 19.35 GHz, horizontal polarization, recorded by SSM/I is plotted for cells containing the test site at resolution of 25 km. Microwave brightness temperature at 19.35 GHz is sensitive to the liquid water content within the snowpack (e.g., Tedesco et al., 2007). When snow melts, snow grains tend to bind to each other (constructive metamorphism) with the grain size of melted and/or refrozen snow generally larger than that of unthawed snow.

The comparison between MODIS-retrieved and CROCUS simulated snow grain diameter, and brightness temperature was performed over four selected test sites: Dye-2 (66.4810N, 46.2800W), Saddle (66.0006N, 44.5014W), South Dome (63.1489N, 44.8167W) and NASA SE (66.4797N, 42.5002W). The results are shown in Fig. 6. The MODIS results are averaged over an area of 25×25 km^2 for an easy comparison with SSM/I measurements. Note that CROCUS data are reduced by a factor of two. In this case, there is a good general agreement between CROCUS values and MODIS retrievals for the off-melting season and the first period of strong thaw (June, days 170–176). The best agreement for this period is observed for NASA SE and Saddle sites. For the Dye-2 and South-Dome sites, the maximum of melting is shifted by several days.

Overall, analysis of MODIS results suggests two well-expressed melting periods during the summer of 2004, with the second one occurring in August (days 220–226). One can see that CROCUS overestimates the length of melting period by almost 10 days over Saddle and South-Dome and it fails to predict a strong melting event over site Dye-2. The SSM/I brightness temperature for this period of time supports the results obtained with MODIS.

Between June and August, CROCUS simulations predict additional intermediate high amplitude thawing periods for sites NASA-SE, Saddle and South-Dome, which are not detected with MODIS. Some of the disagreement between MODIS and CROCUS might be caused by cloudiness. Because of the inevitable errors in cloud detection, when cloudy pixels are masked as clear, the developed algorithm may produce lower grain size values in cloudy conditions. On the other hand, SSM/I data, which are not affected by cloudiness, do not support the predicted melting by CROCUS.

6. Seasonal melting over Greenland in 2004

Snow grain size monitoring over the Greenland ice sheet can support development of algorithms for snowmelt detection (e.g. Chylek et al., 2007) and provide additional forcing data for snow models. The MODIS TERRA results for the melting period of 2004 are shown in Fig. 7. Each image is obtained as a 3-day composite to cover gaps caused by clouds with selection of the maximal-value grain size over a 3-day period which helps filter low bias caused by undetected clouds. This compositing procedure may produce some artifacts, such as sharp linear borders in the northern part of Greenland on days 208 and 220. Despite some inner areas remain un-initialized with our retrievals (shown by black color), the images provide a sufficiently good coverage and temporal resolution to detect short periods of melting.

The first image shows results for the middle of April, 2004. Note that we don't currently discriminate sea ice whose reflectance is similar to that of snow in the inner regions of Greenland. In May–June,

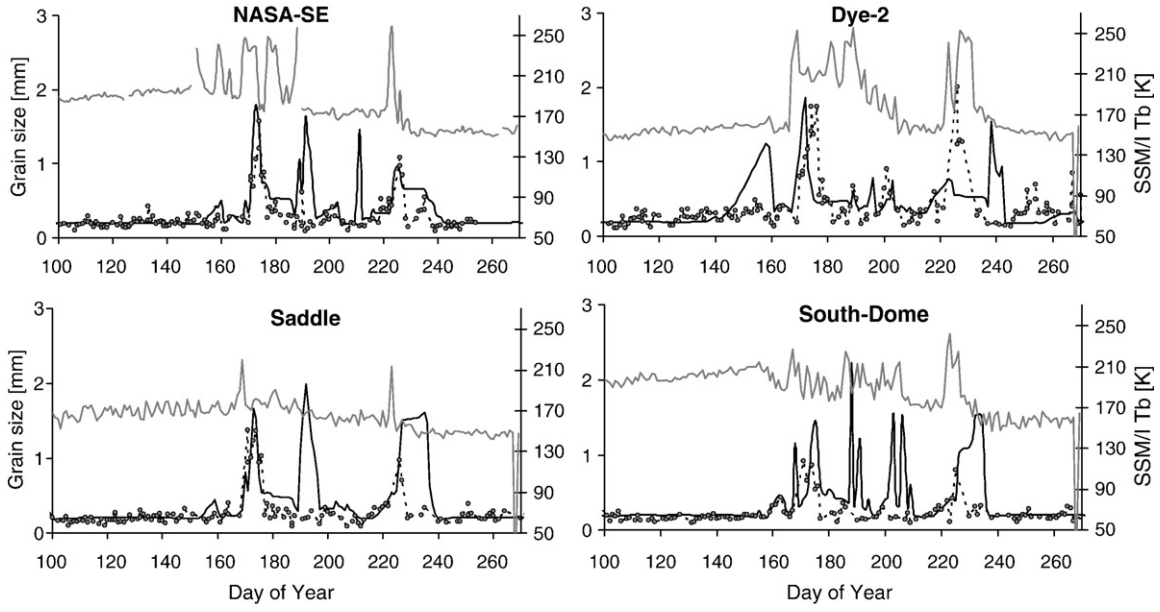

Fig. 6. Comparison of the time series of snow grain size and SSM/I brightness temperature for four sites of Greenland in 2004. The gray line show SSM/I brightness temperature, the solid line shows CROCUS value reduced by a factor of two, and circles connected by a dashed line show MODIS-retrieved snow grain diameter.

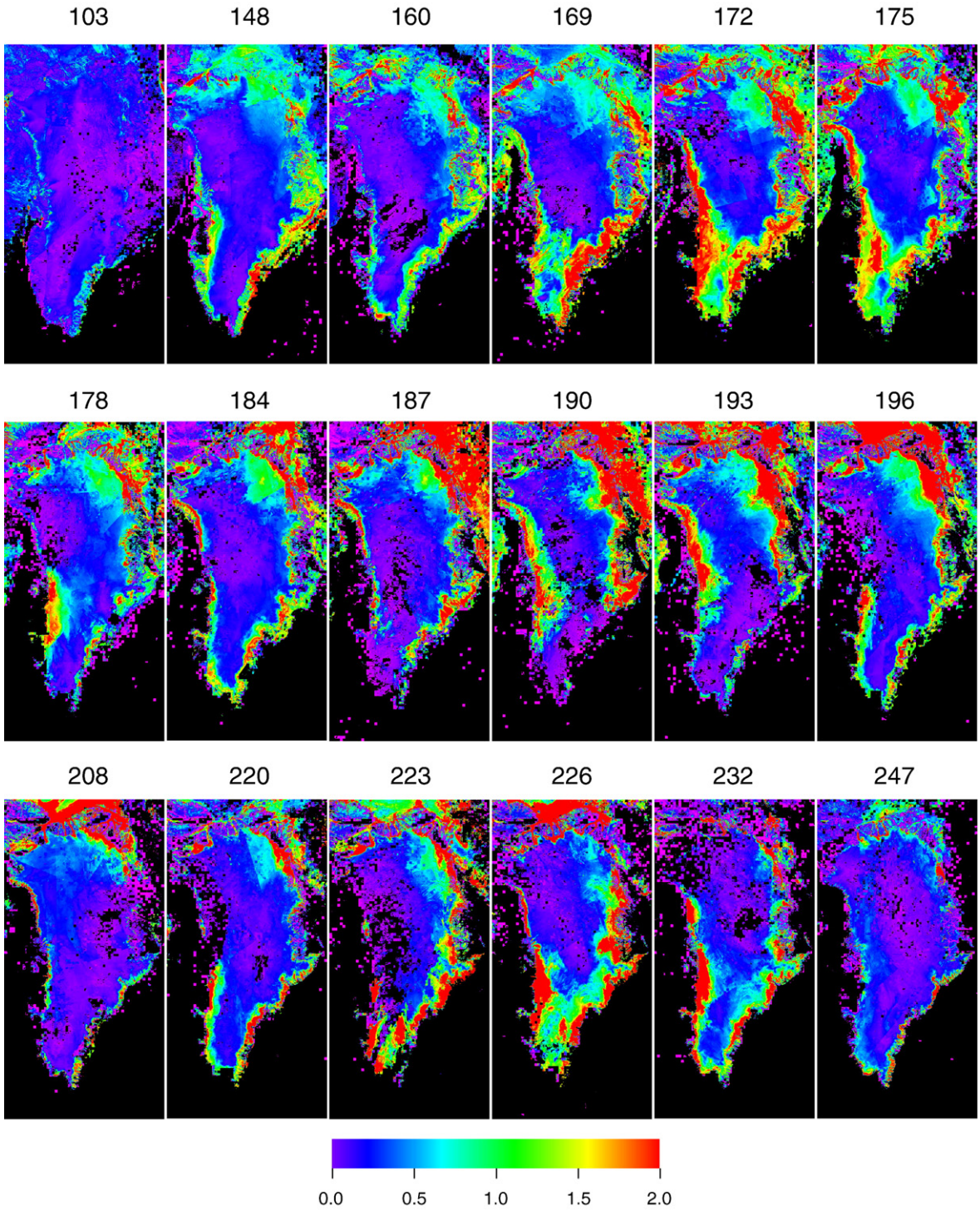

Fig. 7. Snow grain size (mm) retrieved from MODIS TERRA data for the melting period of 2004 over Greenland. Each image is obtained as a 3-day composite to cover gaps caused by clouds.

melting takes place in the peripheral area of Greenland and adjacent sea ice. The red color on the border of the ice sheet indicates high grain size values. On the other hand, a relatively coarse resolution of our data (1 km) may result in undetected presence of pools of pure water cleared from sea ice along the shores, which will also be interpreted as larger snow grains.

Figures for the last week of June (days 169–175) show strong melting in the southern inner region of Greenland as well as melting along the northern and western perimeter of Greenland. The melting largely abates by day 178. In July, melting continues mainly in the north of Greenland. A second period of melting begins in the middle of August. The strip of low values in the middle of southern Greenland on day 223 is probably an artifact as this region was continuously covered by clouds during compositing period.

Despite some artifacts due to compositing and residual cloudiness, the developed algorithm is capable of operationally producing spatial maps of the grain size over Greenland of a good quality without additional filtering or compositing techniques. This can be established

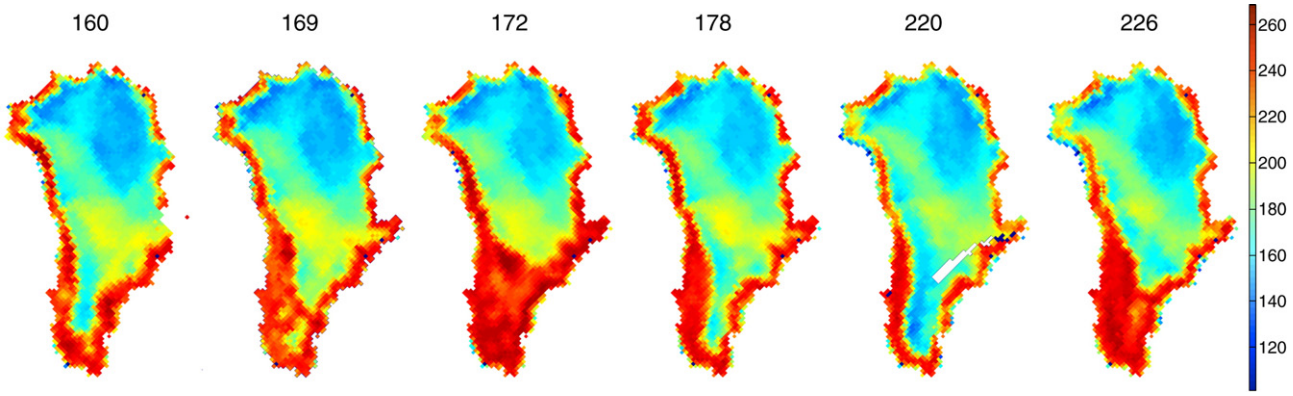

Fig. 8. SSM/I brightness temperature over Greenland for 2004.

qualitatively by comparing our results with maps of microwave brightness temperature. Fig. 8 shows SSM/I brightness temperature images for selected days of 2004. The low brightness temperature values characterize areas of dry snow whereas relatively high values indicate presence of wet snow. A visual comparison between MODIS retrievals and microwave data shows a good spatial agreement for the periods and spatial extent of melting.

7. Conclusions

Snow grain size is an important parameter which knowledge is required in various disciplines, from snow chemistry of gases to the Earth radiation balance. The grain size along with snow temperature and soot concentration was an operational product of the Global Imager aboard ADEOS-II satellite (Hori et al., 2007) during its mission in 2003. In this paper, we described a new algorithm with operational capabilities to derive snow grain size from MODIS data over Greenland.

The new algorithm uses the framework of MAIAC processing to detect clouds, retrieve water vapor and perform atmospheric correction of MODIS measurements. Cloud discrimination over bright snow and ice surfaces is a very difficult problem, and robust performance of MAIAC cloud mask algorithm is a key to successful retrieval of snow properties.

The grain size retrieval is based on the AART model which predicts analytically the spectral and directional snow reflectance as an explicit function of snow grain size and absorption within the snowpack. We took advantage of the analytical form of solution to develop an explicit and fast retrieval algorithm using the ratio of MODIS measurements in bands 5 (1.24 μm) and 1 (0.645 μm). Additional retrievals in the SWIR bands 6 (1.6 μm) and 7 (2.11 μm) with higher snow absorption and lower light penetration depth can potentially be used to evaluate vertical profile of grain size (Li et al., 2001). The consistency of solution was demonstrated over the full range of the MODIS TERRA viewing geometries in daytime conditions, excluding the forward scattering (glint) range of azimuthal angles ($\varphi \leq 40°$) where the AART model is not valid. We also demonstrated consistency of the time series of retrieved grain size and a good sensitivity of the algorithm to detect snowmelt and at least some of the snow precipitation events.

The retrieval method was validated with snow pit measurements of Aoki et al. (2007) collected over Barrow, Alaska and Hokkaido, Japan in 2001–2005. The retrievals are shown to have a good correlation with measurements for the range of snow diameters ~0.1–1 mm. At the same time, this comparison revealed that the AART model may need a calibration factor of ~1.5 to achieve a quantitative agreement between the derived optical grain size and the physical value. This conclusion is very preliminary given the discussed uncertainties of the ground measurements, and further work is needed to achieve a reliable snow model calibration.

The results of retrievals were also compared for the year of 2004 with microwave brightness temperature of SSM/I radiometer which is sensitive to the amount of liquid water in snow. The Greenland-scale comparisons show a good agreement in detection of two main melting periods in 2004, in the middle of June and in August. We believe that MODIS-based retrievals may have a better sensitivity to the changes in snow metamorphism than the microwave measurements, in part due to significantly better spatial resolution (1 km vs 25 km), though temporal resolution might be affected by clouds.

MODIS retrievals were also compared with the snow model CROCUS driven with surface meteorological data recorded on ground by the Greenland Climate Network automatic stations for four different selected sites. Overall, the comparison was satisfactory although the grain size of CROCUS is found to be on average a factor of two larger, which generally agrees with the finding from the direct validation (a factor of ~1.5). CROCUS also showed a higher number of predicted periods of thaw. There are certain differences in the magnitude and longevity of the main melting periods as well. The independent SSM/I results agree much better with MODIS retrievals than with CROCUS prediction results.

The current algorithm is fast and can be run operationally ensuring robust performance over Greenland. On the other hand, our processing model needs some further development. We plan to include the light absorption by snow impurities, such as soot, in order to adapt the algorithm for the regions with high urban impact on snow. An enhancement is needed to discriminate sea ice based on MODIS data and fine-tune MAIAC cloud mask for the Arctic environment. We demonstrated a sensitivity of method to detect fresh snowfall but further work is needed to get to the point of automated classification of such events. One important part of future research is development of a theoretical model to account for surface roughness which would bring the model to an agreement with measurements which show a systematically lower anisotropy of snow reflectance (function R_0). In this sense, a combination of MODIS with high frequency of observations over polar regions with multi-angle capabilities of MISR onboard EOS TERRA would be an excellent source of experimental test data with wide angular coverage.

Acknowledgement

The work of Dr. Lyapustin and Dr. Wang was supported by the NASA EOS Science (Dr. D. Wickland) and NPP (Dr. J. Gleason) grants. The work of A. Kokhanovsky was supported by ESA Project “Snow Radiance”. The authors would like to thank the reviewers for deep and insightful comments.

References

Aoki, T., Aoki, T., Fukabori, M., Hachikubo, A., Tachibana, Y., & Nishio, F. (2000). Effects of snow physical parameters on spectral albedo and bidirectional reflectance of snow surface. *Journal of Geophysical Research*, *105*(D8), 10219−10236.

Aoki, T., Aoki, T., Fukabori, M., Tachibana, Y., Zaizen, Y., Nishio, F., et al. (1998). Spectral albedo observation on the snow field at Barrow, Alaska. *Polar Meteorology and Glaciology*, *12*, 1—9.

Aoki, T., Hori, M., Motoyoshi, H., Tanikawa, T., Hachikubo, A., Sugiura, K., et al. (2007). ADEOS-II/GLI snow/ice products — Part II: Validation results using GLI and MODIS data. *Remote Sensing of Environment*, *111*, 274—290.

Bentley, W. A. (1931). *Snow crystals*, 1st ed. McGraw-Hill. 227 pp.

Bodhaine, B. A., Wood, N. B., Dutton, E. G., & Slusser, J. R. (1999). On Rayleigh optical depth calculations. *Journal of Atmospheric and Oceanic Technology*, *16*, 1854—1861.

Brun, E., David, P., Sudul, M., & Brugnot, G. (1992). A numerical model to simulate snow-cover stratigraphy for operational avalanche forecasting. *Journal of Glaciology*, *38*, 13—22.

Brun, E., Martin, E., Simon, V., Gendre, C., & Coleou (1989). An energy and mass model of snow cover suitable for operational avalanche forecasting. *Journal of Glaciology*, *35*, 333—342.

Chylek, P., McCabe, M., Dubey, M. K., & Dozier, J. (2007). Remote sensing of Greenland ice sheet using multi-spectral near-infrared and visible radiances. *Journal of Geophysical Research*, *112*, D24S20. doi:10.1029/2007JD008742

Colbeck, S. C. (1983). Theory of metamorphism of dry snow. *Journal of Geophysical Research*, *88*(C9), 5475—5482.

Domine, F., Albert, M., Huthwelker, T., Jacobi, H. -W., Kokhanovsky, A. A., Lehning, M., et al. (2008). Snow physics as relevant to snow photochemistry. *Atmospheric Chemistry and Physics*, *8*, 171—208.

Frank, F. C. (1974). Descartes' observations on the Amsterdam snowfalls of 4, 5, 6 and 9 February 1634. *Journal of Glaciology*, *13*, 535.

Green, R. O., Dozier, J., Roberts, D. A., & Painter, T. H. (2002). Spectral snow reflectance models for grain size and liquid water fraction in melting snow for the solar reflected spectrum. *Annals of Glaciology*, *34*, 71—73.

Grenfell, T. C., Warren, S. G., & Mullen, P. C. (1994). Reflection of solar radiation by the Antarctic snow surface at ultraviolet, visible, and near-infrared wavelengths. *Journal of Geophysical Research*, *99*(D9), 18669—18684.

Hooke, R. (2003). *Micrographia.* Courier Dover Publications ISBN 0486495647, 384 pp.

Hori, M., Aoki, T., Stamnes, K., & Li, W. (2007). ADEOS-II/GLI snow/ice products — Part III: Retrieved results. *Remote Sensing of Environment*, *111*, 291—336.

Hudson, S. R., & Warren, S. G. (2007). An explanation for the effect of clouds over snow on the top-of-atmosphere bidirectional reflectance. *Journal of Geophysical Research*, *111*(D18). doi:10.1029/2007/JD008541

Hudson, S. R., Warren, S. G., Brandt, R. E., Grenfell, T. C., & Six, D. (2006). Spectral bidirectional reflectance of Antarctic snow: Measurements and parameterization. *Journal of Geophysical Research*, *112*(D19202). doi:10.1029/2006/JD007290

Kepler, J. (1611). *The six-cornered snowflake, translated by L. L. Whyte.* Oxford Univ. Press 1966.

Kneizys, F. X., Abreu, L. W., Anderson, G. P., Chetwynd, J. H., Shettle, E. P., Berk, A., et al. (1996). The MODTRAN 2/3 report and LOWTRAN 7 model. *MODTRAN Report* North Andover, MA: Ontar Corporation. 261 pp.

Kokhanovsky, A. A. (2006). *Cloud optics.* Berlin: Springer.

Kokhanovsky, A. A. (2006). Scaling constant and its determination from simultaneous measurements of light reflection and methane adsorption by snow samples. *Optics Letters*, *31*, 3282—3284.

Kokhanovsky, A. A., Aoki, T., Hachikubo, A., Hori, M., & Zege, E. P. (2005). Reflective properties of natural snow: Approximate asymptotic theory versus in situ measurements. *IEEE Transactions on Geoscience and Remote Sensing*, *43*, 1529—1535.

Kokhanovsky, A., & Zege, E. P. (2004). Scattering optics of snow. *Applied Optics*, *43*, 1589—1602.

Kokhanovsky, A. A., & Schreier, M. (2009). The determination of specific snow area, albedo, and the effective grain size using AATSR spaceborne observations. *International Journal of Remote Sensing*, *30*, 919—933.

Li, W., Stamnes, K., Chen, B., & Xiong, X. (2001). Retrieval of the depth dependence of snow grain size from near-infrared radiances at multiple wavelengths. *Geophysical Research Letters*, *28*, 1699—1702.

Lyapustin, A. I. (1999). Atmospheric and geometrical effects on land surface albedo. *Journal of Geophysical Research*, *104*, 4123—4143.

Lyapustin, A. (2003). Interpolation and Profile Correction (IPC) method for shortwave radiative transfer in spectral intervals of gaseous absorption. *Journal of the Atmospheric Sciences*, *60*, 865—871.

Lyapustin, A. (2005). Radiative transfer code SHARM for atmospheric and terrestrial applications. *Applied Optics*, *44*, 7764—7772.

Lyapustin, A., & Wang, Y. (2008). MAIAC: Multi-angle implementation of atmospheric correction for MODIS. *Algorithm Theoretical Basis Document*, *Vol. 1.* 77 pp., available at http://neptune.gsfc.nasa.gov/bsb/subpages/index.php?section=Projects&content=MAIAC%20ATDB

Lyapustin, A., & Wang, Y. (2009). The time series technique for aerosol retrievals over land from MODIS. In A. Kokhanovky & G. De Leeuw (Eds.), *Satellite aerosol remote sensing over land* (pp. 69—99). Springer Praxis Books ISBN 978-3-540-69396-3.

Lyapustin, A., Wang, Y., & Frey, R. (2008). An automatic cloud mask algorithm based on time series of MODIS measurements. *Journal of Geophysical Research*, *113*, D16207. doi:10.1029/2007JD009641

Mie, G. (1908). Bitrage zur Optik truber Medien speziell kolloidaler Metallosungen. *Annalen der Physik*, *25*, 377—445.

Mishchenko, M. I., Dlugach, J. M., Yanovitskij, E. G., & Zakharova, N. T. (1999). Bidirectional reflectance of flat, optically thick particulate layers: An efficient radiative transfer solution and applications to snow and soil surfaces. *Journal of Quantitative Spectroscopy & Radiative Transfer*, *63*, 409—432.

Mlawer, E. J., Tobin, D. C., & Clough, S. A. (in preparation). A revised perspective on the water vapor continuum: The MT_CKD Model.

Nakaya, U. (1954). *Snow crystals: Natural and artificial.* Harvard University Press.

Nolin, A. W., & Dozier, J. (1993). Estimating snow grain size using AVIRIS data. *Remote Sensing of Environment*, *44*, 231—238.

Nolin, A. W., & Dozier, J. (2000). A hyperspectral method for remotely sensing the grain size of snow. *Remote Sensing of Environment*, *74*, 207—216.

Nolin, A. W., & Payne, M. C. (2007). Classification of glacier zones in western Greenland using albedo and surface roughness from the Multi-Angle Imaging Spectro-Radiometer (MISR). *Remote Sensing of Environment*, *107*, 264—275.

Painter, T. H., Dozier, J., Roberts, D. A., Davis, R. E., & Greene, R. O. (2003). Retrieval of subpixel snow-covered area and grain size from imaging spectrometer data. *Remote Sensing of Environment*, *85*, 64—77.

Rothman, L. S., Barbe, A., Benner, D. C., Brown, L. R., Camy-Peyret, C., Carleer, M. R., et al. (2003). The HITRAN molecular spectroscopic database: Edition of 2000 including updates through 2001. *Journal of Quantitative Spectroscopy & Radiative Transfer*, *82*, 5—44.

Scambos, T. A., Haran, T. M., Fahnestock, M. A., Painter, T. H., & Bohlander, J. (2007). MODIS-based mosaic of Antarctica (MOA) data sets: Continent-wide surface morphology and snow grain size. *Remote Sensing of Environment*, *11*, 242—257.

Stamnes, K., Li, W., Eide, H., Aoki, T., Hori, M., & Storvold, R. (2007). ADEOS-II/GLI snow/ice products — Part I: Scientific Basis. *Remote Sensing of Environment*, *111*, 258—273.

Steffen, K., Box, J. E., & Abdalati, W. (1996). Greenland climate network: GC-Net. In S. C. Colbeck (Ed.), *CRREL 96-27 special report on glaciers, ice sheets and volcanoes, trib. to M. Meier* (pp. 98—103).

Tedesco, M. (2007). Snowmelt detection over the Greenland ice sheet from SSM/I brightness temperature daily variations. *Geophysical Research Letters*, *34*, L02504. doi:10.1029/2006GL028466

Tedesco, M. (2007). A new record in 2007 for melting in Greenland. *EOS*, *88*(39), 383.

Tedesco, M., Abdalati, W., & Zwally, H. J. (2007). Persistent surface snowmelt over Antarctica (1987–2006) from 19.35 GHz brightness temperatures. *Geophysical Research Letters*, *34*, L18504. doi:10.1029/2007GL031199

Tedesco, M., & Kokhanovsky, A. (2007). The semi-analytical snow retrieval algorithm and its application to MODIS data. *Remote Sensing of Environment*, *111*, 228—241.

Tomasi, C., Vitale, V., Lupi, A., Campanelli, M., Herber, A., Treffeisen, R., et al. (2007). Aerosols in polar regions: A historical overview based on optical depth and in situ observations. *Journal of Geophysical Research*, *112*, D16205. doi:10.1029/2007JD008432

Warren, S. G., & Brandt, R. E. (2008). Optical constants of ice from the ultraviolet to the microwave: A revised compilation. *Journal of Geophysical Research*, *113*, D14220. doi:10.1029/2007JD009744

Warren, S. G., & Clarke, A. D. (1986). Soot from Arctic haze: Radiative effects on the Arctic snowpack. *Glaciological Data*, *18*, 73—77.

Wiscombe, W. J., & Warren, S. G. (1980). A model for the spectral albedo for snow. I. Pure snow. *Journal of the Atmospheric Sciences*, *37*, 2712—2733.

Zhou, X., Li, S., & Stamnes, K. (2003). Effects of vertical inhomogeneity on snow spectral albedo and its implication for optical remote sensing of snow. *Journal of Geophysical Research*, *108*, 4738. doi:10.1029/2003JD003859